

Parallel Electron-Hole Bilayer Conductivity from Electronic Interface Reconstruction

R. Pentcheva,¹ M. Huijben,² K. Otte,¹ W. E. Pickett,³ J. E. Kleibeuker,² J. Huijben,² H. Boschker,² D. Kockmann,² W. Siemons,⁴ G. Koster,² H. J. W. Zandvliet,² G. Rijnders,² D. H. A. Blank,² H. Hilgenkamp,² and A. Brinkman²

¹*Department of Earth and Environmental Sciences, University of Munich, D-80333 Munich, Germany*

²*MESA⁺ Institute for Nanotechnology, University of Twente, 7500 AE Enschede, The Netherlands*

³*Department of Physics, University of California, Davis, California 95616, USA*

⁴*Department of Physics, University of California, Berkeley, California 94720, USA*

(Received 22 December 2009; published 23 April 2010)

The perovskite SrTiO₃-LaAlO₃ structure has advanced to a model system to investigate the rich electronic phenomena arising at polar oxide interfaces. Using first principles calculations and transport measurements we demonstrate that an additional SrTiO₃ capping layer prevents atomic reconstruction at the LaAlO₃ surface and triggers the electronic reconstruction at a significantly lower LaAlO₃ film thickness than for the uncapped systems. Combined theoretical and experimental evidence (from magnetotransport and ultraviolet photoelectron spectroscopy) suggests two spatially separated sheets with electron and hole carriers, that are as close as 1 nm.

DOI: 10.1103/PhysRevLett.104.166804

PACS numbers: 73.20.-r, 71.30.+h, 71.35.-y, 77.55.-g

Polarity discontinuities at the interfaces between different crystalline materials are usually compensated by atomic reconstructions via defects or adsorbates as in conventional semiconductor interfaces. However, in complex oxides the mixed valence states provide an extra option for charge rearrangement by redistributing electrons at lower energy cost than redistributing ions. The remarkable electronic transport properties that occur at the interface between the band insulators SrTiO₃ (STO) and LaAlO₃ (LAO) [1–8] have been attributed to this so called electronic reconstruction [9,10] but direct evidence has not yet been found.

The polarity of LAO arises from the LaO and AlO₂ layers being not charge neutral in the [001] direction, unlike the formally neutral TiO₂ and SrO layers of STO. In the ionic limit, LaO has a charge $q = +e$ and AlO₂ $q = -e$ per unit cell. The screened dipole per unit cell is then $D = q\Delta z/\epsilon$, where the spacing $\Delta z = c/2$ ($c = 3.9 \text{ \AA}$ is the out of plane lattice parameter) and $\epsilon = 25$ is the dielectric constant of LAO [11]. Screening contributions come primarily from a strong lattice polarization of the LAO film (their contribution can be as high as $\sim 62\%$ [12]), supplemented by electronic cloud deformation [13]. For STO-LAO systems, the remaining screened dipole of 0.08 e\AA per cell is expected to give rise to an internal electric field of $2.4 \times 10^7 \text{ V/cm}$, and a resulting buildup of electric potential of 0.9 V per LAO unit cell.

This potential shift explains quantitatively why, above a threshold of 3–4 unit cells, electrons are transferred from the surface, across the LAO slab, into the STO conduction band. The resulting insulator-to-metal transition has been observed experimentally for the n -type LaO/TiO₂ interface [4]. However, the corresponding potential shifts across LAO have not been detected so far in experiments [14], which suggests that possibly nonelectronic reconstructions occur during the growth. To avoid potential buildup also

the LAO surface itself needs to reconstruct, either structurally, electronically, or chemically. After electronic charge transfer one would expect holes at the surface, which have also never been observed.

In this Letter we show that an additional STO capping layer circumvents structural and chemical reconstructions at the LAO surface. The O $2p$ band in the STO capping layer allows for hole doping, so that an electronic reconstruction mechanism comes into play. By means of the STO capping layer one enters a new regime in the field of electronically reconstructed oxide interfaces with two spatially separated 2D conducting sheets, one electronlike and the other holelike, that can display new electronic behavior including the possibility of a 2D excitonic liquid phase.

The system consisting of a varying number of LAO monolayers (ML), $n = 1\text{--}5$ ML, and of a STO capping layer, $m = 0\text{--}2$ ML, stacked on an STO(001) substrate, was studied by density functional theory (DFT) calculations in the generalized gradient approximation (GGA) (for details see Refs. [12,15]). The calculated layer-resolved densities of states are presented in Fig. 1(a) for 2 ML LAO with and without 1 ML STO capping. The effect of the electric field within the LAO film is apparent from the shifts of bands, e.g., by $\sim 0.4 \text{ eV}$ per LAO unit-cell for the uncapped system [12]. Note, that this potential shift is smaller than the mentioned 0.9 eV due to effects related to the well-known underestimation of band gaps by DFT.

Adding a single unit-cell STO capping layer is found to have a dramatic impact on the calculated electronic structure: the band gap, being 1.2 eV for STO(001)/2LAO, is nearly closed for STO(001)/2LAO/1STO. While the ionic relaxation pattern [12] changes significantly when a capping layer is added [15], the net contribution of the buckled TiO₂ and SrO layers does not affect appreciably the total ionic dipole moment of the film (which scales with the

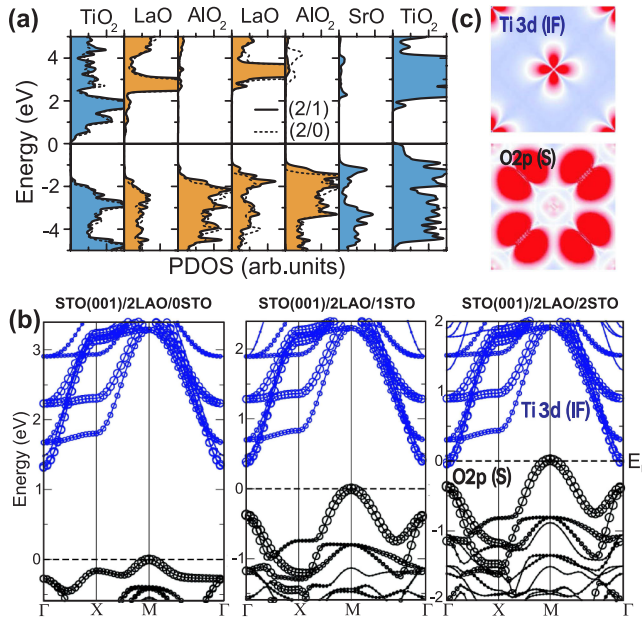


FIG. 1 (color online). (a) Layer-resolved density of states (DOS) of STO(001)/2LAO (dotted line), and STO(001)/2LAO/1STO (black line, colored area) aligned at the bottom of the Ti 3d band at the interface. (b) Influence of $m = 0-2$ STO capping layers on the band structure of STO(001)/2LAO/ m STO. The band gap closes due to overlap between surface O 2p states (black circles) and interface Ti 3d states (blue circles). (c) The electron density for the $m = 2$ system, integrated between -0.6 and 0.0 eV, shows electrons in the Ti 3d_{xy} orbitals at the interface (top) and holes in the O 2p _{π} bands at the surface (bottom).

number of LAO layers). Hence, the gap reduction has mainly an electronic origin.

The evolution of the band structure of STO(001)/2LAO/ m STO with increasing number of capping layers is depicted in Fig. 1(b). The valence band maximum is defined by the O 2p states at the $M(\pi, \pi)$ point in the surface layer, while Ti 3d states at Γ at the n -type interface mark the bottom of the conduction band. In the capped systems a dispersive O 2p surface band extends 0.8 eV above the subsurface O 2p band and effectively reduces the band gap driving the insulator-to-metal transition at an LAO thickness of only 2 ML compared to 4 ML in the uncapped case. This surface state is analogous to the one on the clean STO (001) surface [16,17]. Further STO layers (e.g., STO(001)/2LAO/2STO [15]) increase the band overlap at the Fermi level, but have an overall weaker influence due to the lack of internal field in STO. The reduction of the band gap, and finally its closing, is thus due to three *electronic* effects: (i) the steady upward shift of the O 2p states as they approach the surface [12] due to the internal polarity of LAO, (ii) the band discontinuity at the interface between LAO and the capping STO layer, and (iii) the dispersive O 2p surface band in the capped systems that extends 0.8 eV above the subsurface O 2p band.

Experimentally, we confirm the crucial influence of a single monolayer of nonpolar material on the electronic

interface reconstruction. STO(001)/ n LAO/ m STO samples were made by pulsed laser deposition of n ML of LAO and m ML of STO on TiO₂-terminated STO(001) substrates (for fabrication details, see Refs. [3,6]). While uncapped STO(001)/2LAO samples are found to be insulating (sheet resistance above $1 \text{ G}\Omega/\square$), samples with an additional single ML of STO are conducting [see Fig. 2(a)]. The conductivity is further enhanced in STO(001)/2LAO/2STO samples, but the influence of increasing the STO capping layer thickness weakens, as expected from the DFT results: the STO(001)/2LAO/10STO sample has almost the same conductivity as the STO(001)/2LAO/2STO sample. Samples with a single ML of LAO were found to be insulating except for the sample with a thick STO capping ($m \geq 10$).

It is known that the sheet resistance in STO/LAO samples depends critically on the oxygen pressure during growth [6,18–21] and can vary over many orders of magnitude [6]. Figure 2(b) shows the sheet resistance for two different sets of STO/LAO/STO heterostructures with varying LAO interlayer thickness, grown at a relatively high oxygen pressure (2×10^{-3} mbar) and at lower oxygen pressure (3×10^{-5} mbar). For the coupled-interface samples, the influence of the oxygen pressure is now found to be much weaker. Apparently, the STO capping protects the underlying LAO surface against reconstruction via defects or adsorbates.

In order to obtain spectroscopic evidence for the *electronic* reconstruction, ultraviolet photoelectron spectroscopy (UPS) was performed *in situ* immediately after the growth of a STO(001)/2LAO/1STO sample. Figure 3(a)

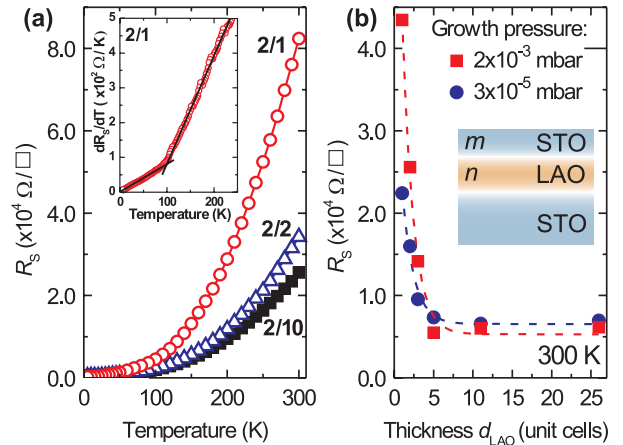


FIG. 2 (color online). (a) Sheet resistance as a function of temperature for STO(001)/2LAO/1STO (red circles), STO(001)/2LAO/2STO (blue triangles), and STO(001)/2LAO/10STO (black squares). All samples are grown at 2×10^{-3} mbar of oxygen. Inset: dR_s/dT as function of temperature with different linear fits below and above 100 K. (b) Sheet resistance at room temperature of STO(001)/ n LAO/10STO samples for varying n LAO thickness and a fixed number of 10 unit cells of STO capping. Red squares/blue circles correspond to oxygen pressure of 2×10^{-3} mbar/ 3×10^{-5} mbar during growth.

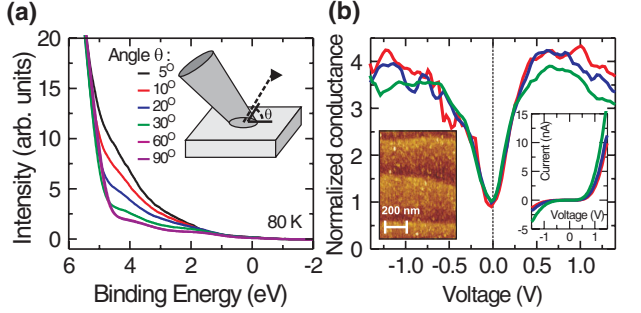


FIG. 3 (color online). (a) UPS spectra of a STO(001)/2LAO/1STO sample taken at 80 K *in situ* after growth under various detector angles (the inset shows how the angle towards the detector is defined). A gradual filling of the valence band towards the Fermi energy is found in the surface-sensitive lower angle spectra. (b) STS conductance $(dI/dV)/(I/V)$ at 300 K for different tip-sample distances (current set-point, respectively, 1.5, 2.0, and 4.0 nA at a bias voltage of -1.5 V). Right inset: I/V curve; left inset shows an STM image recorded at -1.0 V and 300 K.

shows a gradual increase in intensity for the more surface sensitive measurements at lower detector angles. These states originate from the valence band of LAO as well as the valence band of the STO surface ML. Note, that the valence band states penetrate all the way to E_F , unlike studies on doped STO [22], where only trapped states close to the conduction band are usually observed.

To probe states around the Fermi level, scanning tunneling spectroscopy (STS) was performed in ultra high vacuum using a variable temperature cryostat. Figure 3(b) shows the local DOS, $(dI/dV)/(I/V)$, of a STO(001)/2LAO/1STO sample. At room temperature, the Fermi energy lies between the valence band of the STO surface and the conduction band of the substrate-LAO interface. The bandgap is (almost) closed, as predicted in Fig. 1 by DFT (see also [15]). The observed density of states just below E_F , as measured by both UPS and STS, is consistent with the electronic reconstruction scenario and suggests the presence of holes in transport.

To explore the nature of charge carriers in capped systems, magnetoresistance and Hall data were analyzed. Because the intrinsic coupling between the layers would not allow us to probe the transport properties of the layers individually, unless structures are realized on a submicron length scale, our measurements contain information on the layers in parallel. Figure 4 displays a positive nonquadratic magnetoresistance and a Hall resistance whose slope increases for higher fields for all conducting STO/LAO/STO samples. Quantum oscillations can still be excluded because of the low mobility. A negative magnetoresistance contribution, observed for single-interface samples deposited at high oxygen pressure [6], only appears below 10 K. It is natural to interpret the observations in terms of multi-band conductivity. Indeed, in the temperature range up to 100 K, the magnetoresistance as well as the Hall resistance can be fitted with a two-band model [15] [solid lines in

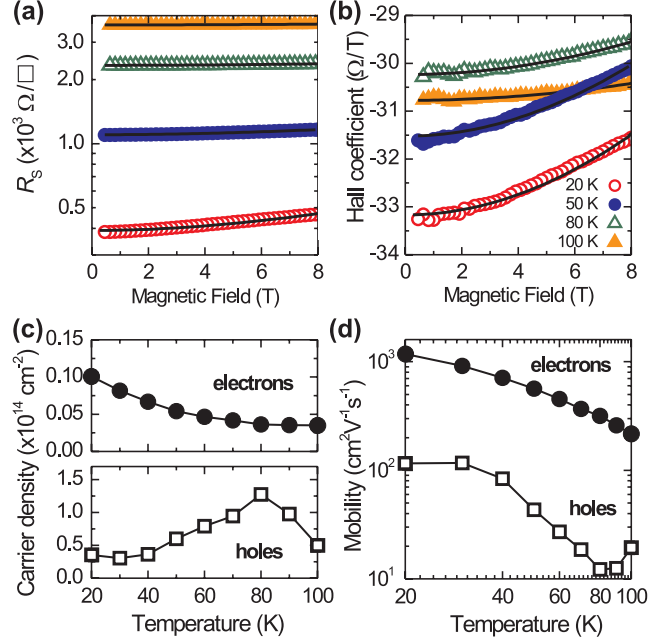


FIG. 4 (color online). (a) Sheet resistance and (b) Hall coefficient (R_H/H) as a function of magnetic field at different temperatures for a STO(001)/2LAO/1STO sample. (c) Sheet carrier densities and (d) mobilities as obtained from a two-band fit to the magnetoresistance and Hall data at each temperature.

Figs. 4(a) and 4(b)]. Two carrier concentrations and two mobilities could be obtained for the STO(001)/2LAO/1STO sample from fitting as a function of temperature [Figs. 4(c) and 4(d)].

The positive carrier sign of one of the bands at low temperatures indicates hole-type conductivity, while the other band is of electron-type. We note that no fit to the data could be obtained for equal signs of the two carrier densities. Neither oxygen vacancy doping, nor doping by cation substitution, have ever been shown to give rise to hole conductivity in the STO/LAO system. The calculated electron density distribution in Fig. 1(c) displays electrons of Ti $3d_{xy}$ orbital character in the interface TiO_2 layer, while holes of O $2p_\pi$ type are present in the surface TiO_2 layer. Consequently, we attribute the hole band to the surface layer, while the electron band, with a lower carrier density but a much larger mobility, is naturally attributed to the Ti $3d_{xy}$ states at the interface to the substrate, consistent with the observations in Ref. [23].

Note, that the hole density is about an order of magnitude larger than the electron density. However, the Hall effect is dominated by the electron band because of its large mobility ($10^3 \text{ cm}^2 \text{ V}^{-1} \text{ s}^{-1}$). The unequal number of electrons and holes illustrates that not all charge carriers are visible in transport measurements. While the effective electron and hole masses cannot be directly inferred from our data, the band structure calculations (neglecting strong correlation effects and defects) render $0.4m_e$ for the electrons (both in the capped and uncapped system) and a significantly higher effective mass of $1.2m_e$ for the holes.

Above 100 K, neither magnetoresistance, nor a nonlinear Hall resistance were observed, because the mobilities become so low that no magnetoresistance effects are expected any longer ($\mu^2 H^2 \ll 1$ in the two-band equations of [15]). Therefore, no two-band fitting analysis can be performed in this case, and no statement can be done on the presence of electrons and holes.

In the STO(001)/2LAO/1STO sample evidence from different experimental techniques point to an electronic reconstruction mechanism. At the same time, we know that for uncapped thick LAO samples no potential buildup has been observed [14], suggestive of nonelectronic reconstruction scenarios. In order to verify whether it is only the capping that makes a difference, the magnetotransport was studied for a large number of samples with either thicker LAO or thicker capping STO [15]. While for defect-free systems DFT predicts an increase in the band overlap, and hence in the number of electrons and holes, no hole contribution was found experimentally beyond $n = 2$ and $m = 1$. Apparently, during growth structural reconstruction occurs whenever the potential buildup exceeds a few eV. While conductivity arises also in this case, no evidence for pure electronic reconstruction exists any longer. The STO(001)/2LAO/1STO sample might be an example of a system where the potential buildup during growth of just 2 ML of LAO is just not yet large enough for a reconstruction. The subsequent capping ML protects the LAO surface from structural or chemical reconstruction, provides another potential increase (either during growth or cool down), and can accommodate mobile holes, resulting in electronic reconstruction. This conclusion provides guidelines to enhance electronic reconstruction effects in general.

As shown in Fig. 1, the surface valence band has its maximum at the $M = (\pi, \pi)$ zone corner, whereas the substrate-LAO interface conduction band has its minimum at the zone center. This makes the band overlap distant not only in real space (across 12 Å or more, depending on capping layer thickness) but also indirect in momentum. As a practical consequence, an electron at the surface cannot move to the substrate without some mechanism to supply the momentum transfer. The obvious mechanism is via phonons, specifically $M = (\pi, \pi)$ phonons. These are zone boundary optical phonons, which typically lie at a few tens of meV energy. Equilibration of electrons and holes across the LAO slab will be slow at low temperature, but will occur rapidly as soon as optical phonons are excited.

In summary, the STO capping has enabled us to show the presence of holes at electronically reconstructed oxide interfaces. Their mobility is low and it is expected that the holes can become localized or eliminated in uncapped STO/LAO systems more strongly (e.g., by absorbed molecules or other defects). This possibly explains the large sensitivity of uncapped samples to growth conditions and the possibility to manipulate the interface conductivity by an atomic force microscope tip [24,25].

A further consequence of this 2D electron-hole bilayer is that it provides the conditions necessary for formation of a 2D excitonic liquid [26,27] comprised of interacting indirect excitons. In this oxide nanostructure the separation of the 2D electron and hole gases can be varied by the choice of polar material as well as capping material. In analogy to other oxides, such as ZnO [28], it is expected that higher mobilities can be obtained by reducing the defect density. Furthermore, the carrier densities can be tuned by gating, allowing a substantial parameter range to be probed.

This work is supported by the Dutch Foundation for Fundamental Research on Matter (FOM), the Netherlands Organization for Scientific Research (NWO) through VIDI and VICI grants, NANONED, the Bavaria-California Technology Center (BaCaTeC), German Science Foundation (TRR80) and DOE's Computational Materials Science Network, DOE grant DE-FG02-04ER46111, NSF grant PHY05-51164, and a grant for computational time at the Leibniz Rechenzentrum.

-
- [1] A. Ohtomo and H. Y. Hwang, *Nature (London)* **427**, 423 (2004); **441**, 120 (2006).
 - [2] N. Nakagawa, H. Y. Hwang, and D. A. Muller, *Nature Mater.* **5**, 204 (2006).
 - [3] M. Huijben *et al.*, *Nature Mater.* **5**, 556 (2006).
 - [4] S. Thiel *et al.*, *Science* **313**, 1942 (2006).
 - [5] N. Reyren *et al.*, *Science* **317**, 1196 (2007).
 - [6] A. Brinkman *et al.*, *Nature Mater.* **6**, 493 (2007).
 - [7] A. D. Caviglia *et al.*, *Nature (London)* **456**, 624 (2008).
 - [8] M. Basletić *et al.*, *Nature Mater.* **7**, 621 (2008).
 - [9] R. Hesper *et al.*, *Phys. Rev. B* **62**, 16046 (2000).
 - [10] S. Okamoto and A. J. Millis, *Nature (London)* **428**, 630 (2004).
 - [11] S. A. Hayward *et al.*, *Phys. Rev. B* **72**, 054110 (2005).
 - [12] R. Pentcheva and W. E. Pickett, *Phys. Rev. Lett.* **102**, 107602 (2009).
 - [13] S. Ishibashi and K. Terakura, *J. Phys. Soc. Jpn.* **77**, 104706 (2008).
 - [14] Y. Segal *et al.*, *Phys. Rev. B* **80**, 241107(R) (2009).
 - [15] See supplementary material at <http://link.aps.org/supplemental/10.1103/PhysRevLett.104.166804>.
 - [16] S. Kimura *et al.*, *Phys. Rev. B* **51**, 11049 (1995).
 - [17] J. Padilla and D. Vanderbilt, *Surf. Sci.* **418**, 64 (1998).
 - [18] W. Siemons *et al.*, *Phys. Rev. Lett.* **98**, 196802 (2007).
 - [19] G. Herranz *et al.*, *Phys. Rev. Lett.* **98**, 216803 (2007).
 - [20] A. Kalabukhov *et al.*, *Phys. Rev. B* **75**, 121404(R) (2007).
 - [21] M. Huijben *et al.*, *Adv. Mater.* **21**, 1665 (2009).
 - [22] W. Maus-Friedrichs *et al.*, *Surf. Sci.* **515**, 499 (2002).
 - [23] M. Salluzzo *et al.*, *Phys. Rev. Lett.* **102**, 166804 (2009).
 - [24] C. Cen *et al.*, *Nature Mater.* **7**, 298 (2008).
 - [25] C. Cen *et al.*, *Science* **323**, 1026 (2009).
 - [26] L. V. Keldysh and Y. V. Kopaev, *Sov. Phys. Solid State* **6**, 2219 (1965).
 - [27] J. des Cloizeaux, *J. Phys. Chem. Solids* **26**, 259 (1965).
 - [28] A. Tsukazaki *et al.*, *Science* **315**, 1388 (2007).